THE EUROPEAN
PHYSICAL JOURNAL C

Regular Article - Theoretical Physics

Probing the $hc\bar{c}$ coupling at a Future Circular Collider in the electron-hadron mode

J. Hernández-Sánchez[1,2,a] , **C. G. Honorato**[1,b], **S. Moretti**[3,4,c]

[1] Fac. de Cs. de la Electrónica, Benemérita Universidad Autónoma de Puebla, Apartado Postal 1152, 72570 Puebla, Puebla, Mexico
[2] Dual C-P Institute of High Energy Physics, Colima, Mexico
[3] School of Physics and Astronomy, University of Southampton, Highfield, Southampton SO17 1BJ, UK
[4] Particle Physics Department, Rutherford Appleton Laboratory, Chilton, Didcot, Oxon OX11 0QX, UK

Abstract We study the production of a neutral Higgs boson at a Future Circular Collider in the electron-hadron mode (FCC-eh) through the leading process $e^- p \to \nu_e h q$ assuming the decay channel $h \to c\bar{c}$, where h is the Standard Model (SM)-like state discovered at the Large Hadron Collider (LHC). This process is studied in the context of a 2-Higgs Doublet Model Type III (2HDM-III) embedding a four-zero texture in the Yukawa matrices and a general Higgs potential, where both Higgs doublets are coupled with up- and down-type fermions. Flavour Changing Neutral Currents (FCNCs) are well controlled by this approach through the adoption of a suitable texture once flavour physics constraints are taken in account. Considering the parameter space where the signal is enhanced and in agreement with both experimental data and theoretical conditions, we analyse the aforementioned signal by taking into account the most important SM backgrounds, separating c-jets from light-flavour and gluon ones as well as b-jets by means of efficient flavour tagging. We find that the $hc\bar{c}$ coupling strength can be accessed with good significance after a luminosity of 1 ab^{-1} for a 50 TeV proton beam and a 60 GeV electron one, the latter with a 80% (longitudinal) polarisation.

1 Introduction

Since the July 2012 discovery of a Higgs boson, h, with properties very consistent with those predicted by the Standard Model (SM), at the Large Hadron Collider (LHC), by the ATLAS and CMS experiments, spontaneous Electro-Weak Symmetry Breaking (EWSB) resting on a minimal Higgs mechanism is apparently well established. While a mass of 125 GeV is not really an indication for the SM construct being the one responsible for these LHC signals, as m_h is a free parameter in it, the fact that production and decay rates involving couplings to $W^\pm$ and Z bosons as well as t, b, τ and μ fermions have been measured and are compatible with the SM genuine predictions (once m_h is measured) is a strong sign in flavour of such a minimal Higgs construct.

However, a notable absence in the list of the SM-like Higgs couplings so far measured is the one involving the $hc\bar{c}$ vertex, which is presently unconstrained. The reason is that corresponding signals at the LHC are masked by an enormous QCD background. In fact, not even the ability to tag c-jets, on a similar footing with what has successfully been done for b-jets, is sufficient to enable a measurement of the Yukawa coupling to c-(anti)quarks at a level comparable to the case of b-ones, as the displaced vertex associated to semi-leptonic c-meson decays is much closer to the interaction point (where the gluon and light flavour jet backgrounds originates) than the one stemming from the corresponding b-meson transitions. Another drawback is that the strength of the $hc\bar{c}$ vertex in the SM is much smaller than that of the $hb\bar{b}$ vertex, as they scale with the fermion mass, which in turn means that the Branching Ratios (BRs) for $h \to c\bar{c}$ is $(m_c/m_b)^2$ times smaller than BR($h \to b\bar{b}$), see, e.g., Ref. [1]. On the other hand, the precise evaluation of decay width $h \to c\bar{c}$ has been studied recently at next-to-next-to-leading order QCD (including the flavour-singlet contribution) and the next-to-leading order electroweak [2].

However, there exist extensions of the SM in which the Higgs sector is enlarged by additional (pseudo)scalar multiplets (singlets, doublets, triplets, etc.), where the $h \to c\bar{c}$ rate can be increased substantially. Herein, owing to the fact

[a] e-mail: jaime.hernandez@correo.buap.mx (corresponding author)

[b] e-mail: carlosg.honorato@correo.buap.mx

[c] e-mail: s.moretti@soton.ac.uk

that the SM-like Higgs discovered at the LHC has a clear doublet nature, we focus on the simplest extension of the SM involving such Higgs multiplet, the so-called 2-Higgs Doublet Model (2HDM). The latter comes in several guises, known as Type I, II, III (or Y) and IV (or X), wherein Flavour Changing Neutral Currents (FCNCs) mediated by (pseudo)scalars can be eliminated under discrete symmetries [3–9], entirely if the latter are exact or sufficiently to comply with experimental limits if they are softly broken. In fact, another, very interesting kind of 2HDM is the one where FCNCs can be controlled by a particular texture in the Yukawa matrices [10]. In particular, in previous papers, we have implemented a four-zero texture, in a scenario which we have called 2HDM Type III (2HDM-III) [11]. This model has a phenomenology that is very rich, which we studied at colliders in various instances [12,13], and some very interesting aspects, like flavour-violating quarks decays, which can be enhanced for neutral Higgs bosons with intermediate mass (i.e., below the top quark mass). In particular, we have studied the signal $\phi_i^0 \to s\bar{b} + h.c.$ ($\phi_i^0 = h, H$) [14,15]. Furthermore, in this model, the parameter space can avoid the current experimental constraints from flavour and Higgs physics and a light charged Higgs boson is allowed [16], so that the decay $H^- \to b\bar{c}$ is enhanced and its BR can be dominant [17,18].

In fact, the 2HDM-III is also an ideal candidate in providing enhanced $h \to c\bar{c}$ rates, as the Yukawa texture parameters that affect the aforementioned $H^\pm$ signatures also enter the $h \to b\bar{b}$ and $h \to c\bar{c}$ ones. In particular, it is always possible to maintain the Yukawa coupling to the b-(anti)quark in the range currently measured at the LHC, and indeed the one foreseen by the end of the High Luminosity LHC (HL-LHC) era [19,20], while enhancing the $h \to c\bar{c}$ one. It is the purpose of this paper to study the scope of the electron-proton Future Circular Collider (FCC-eh), with a Center-of-Mass (CM) energy of 3.5 TeV [21–23]. This configuration is obtained by the collisions of a 50 TeV proton beam coming from the FCC-hh [24] and a 60 GeV electron beam from an external linear accelerator (Electron Recovery Linac (ERL)) tangential to the FCC main tunnel [23] and offers good prospects as a Higgs boson factory, as herein one could elucidate the nature of the couplings of generic Higgs bosons to most fermions, especially the $h \to b\bar{b}$ one, which remains difficult to establish with high precision at both the LHC and the HL-LHC because of the overwhelming QCD background.[1] Given these encouraging results for the $hb\bar{b}$ vertex, we specifically analyse here the prospects of also establishing the $hc\bar{c}$ one.

Our work is organised as follows. In the next section we describe briefly the 2HDM-III, specifically, its Yukawa structure. Then in the following one we discuss the theoretical and experimental constraints applying to it and select some benchmark scenarios for numerical analysis. In Sect. 4 we give our results whereas in Sect. 5 we finally summarise.

2 The Higgs sector of the 2HDM-III

The 2HDM-III is described by two scalar Higgs doublets $\Phi_i = (\phi_i^-, \phi_i^{0*})$ ($i = 1, 2$), with hypercharge $+1$, which can couple to all fermions. FCNCs are controlled by a specific four-zero texture in the Yukawa matrices, the latter being an effective flavour theory of the Yukawa sector. Therefore, a discrete symmetry is not necessary in this approach, so that the $SU(2)_L \times U(1)_Y$ invariant scalar potential in its general form can be considered, which is given by [26–29]:

$$
\begin{aligned}
V(\Phi_1, \Phi_2) =\ & \mu_1^2(\Phi_1^\dagger \Phi_1) + \mu_2^2(\Phi_2^\dagger \Phi_2) \\
& - \left(\mu_{12}^2(\Phi_1^\dagger \Phi_2 + h.c.) \right) \\
& + \frac{1}{2}\lambda_1(\Phi_1^\dagger \Phi_1)^2 + \frac{1}{2}\lambda_2(\Phi_2^\dagger \Phi_2)^2 \\
& + \lambda_3(\Phi_1^\dagger \Phi_1)(\Phi_2^\dagger \Phi_2) + \lambda_4(\Phi_1^\dagger \Phi_2)(\Phi_2^\dagger \Phi_1) \\
& + \left(\frac{1}{2}\lambda_5(\Phi_1^\dagger \Phi_2)^2 + \lambda_6(\Phi_1^\dagger \Phi_1)(\Phi_1^\dagger \Phi_2) \right. \\
& \left. + \lambda_7(\Phi_2^\dagger \Phi_2)(\Phi_1^\dagger \Phi_2) + h.c. \right),
\end{aligned}
\tag{1}
$$

wherein, for simplicity, we suppose that all parameters are real[2] as so are the Vacuum Expectation Values (VEVs) of the Higgs fields. Besides, notice that, when a discrete symmetry is implemented in the model, the $\lambda_{6,7}$ terms are absent. However, in our model, the latter can be kept in the Higgs potential when the four-zero texture is implemented in the Yukawa matrices. This is rather interesting, as we have shown that these parameters ($\lambda_{6,7}$) can be relevant in one-loop processes but do not contribute to EW parameter $\rho = m_W^2/m_Z^2 \cos^2\theta_W$ [30]. However, the ordinary custodial symmetry [3,7] (twisted custodial symmetry [31]) associated to the ρ parameter is broken when the difference $m_{H^\pm} - m_A(m_{H^\pm} - m_H)$ is sizeable, being $H^\pm$ the charged Higgs boson and $A(H)$ the heavy CP-odd(even) one belonging to this construct, in addition to the aforementioned SM-like h state. Reasonable models with such an extended Higgs sector are those for which $\rho \approx 1$ when radiative corrections are included [7,27,31–36] or, more in general, those in good agreement with the experimental constraints from the oblique parameters S, T and U [37,38], part of the so-called EW

---

[1] Other interesting studies for probes of Higgs coupling in Higgs pair production at hadron electron colliders LHeC and FCC-eh have been realised recently [25].

[2] The μ_{12}^2 and λ_i ($i = 5, 6, 7$) parameters could be complex in general, which then induce CP-violation in the Higgs sector.

Table 1 The parameters choices for X, Y and $\varepsilon_h^{u,d}$ of the 2HDM-III needed to obtain the standard 2HDM Type I, II and Y (flipped), which happen when the χs are zero

2HDM-III	X	Y	ε_h^u	ε_h^d
2HDM-I	$-\cot\beta$	$\cot\beta$	$\cos\alpha/\sin\beta$	$\cos\alpha/\sin\beta$
2HDM-II	$\tan\beta$	$\cot\beta$	$\cos\alpha/\sin\beta$	$-\sin\alpha/\cos\beta$
2HDM-Y (flipped)	$\tan\beta$	$\cot\beta$	$\cos\alpha/\sin\beta$	$-\sin\alpha/\cos\beta$

Precision Observables (EWPOs) [39]. The described Higgs bosons spectrum emerges after EWSB, which provide mass to the $W^\pm$ and Z bosons, thus releasing five physical Higgs fields: two CP-even neutral states h, H (with $m_h < m_H$), one CP-odd neutral state A plus two charged Higgs bosons $H^\pm$. Furthermore, one also has the mixing angle α, that relates the two CP-even neutral bosons (h, H) and β (being $\tan\beta$ the ratio of VEVs of the two Higgs doublets). The masses of these Higgs fields and these two angles are the inputs parameters chosen here to describe the scalar potential.

About the Yukawa sector of our model, this is defined by [16]:

$$
\begin{aligned}
\mathcal{L}_Y = -\Big(& Y_1^u \bar{Q}_L \tilde{\Phi}_1 u_R + Y_2^u \bar{Q}_L \tilde{\Phi}_2 u_R \\
& + Y_1^d \bar{Q}_L \Phi_1 d_R + Y_2^d \bar{Q}_L \Phi_2 d_R \\
& + Y_1^l \bar{L}_L \tilde{\Phi}_1 l_R + Y_2^l \bar{L}_L \tilde{\Phi}_2 l_R \Big),
\end{aligned}
\tag{2}
$$

being $\tilde{\Phi}_i = i\sigma_2 \Phi_i^*$ ($i = 1, 2$) and where both Higgs doublets are coupled with up- and down-type fermions. Following the procedure of Refs. [16,40], after EWSB, the fermion mass matrices are:

$$
M_f = \frac{1}{\sqrt{2}}(v_1 Y_1^f + v_2 Y_2^f) \quad (f = u, d, \ell),
\tag{3}
$$

where the Yukawa matrices $Y_{1,2}^f$ have the four-zero texture form and are Hermitian. Considering the diagonalisation of the fermion mass matrices through $\bar{M}_f = V_{fL}^\dagger M_f V_{fL}$, we have $\tilde{Y}_n^f = V_{fL}^\dagger Y_n^f V_{fL}$, then one can get a good approximation for the rotated matrix $\tilde{Y}_n^f$ as follows [16]:

$$
\left(\tilde{Y}_n^f\right)_{ij} = \frac{\sqrt{m_i^f m_j^f}}{v}(\tilde{\chi}^f)_{ij} = \frac{\sqrt{m_i^f m_j^f}}{v}\chi_{ij}^f e^{\theta_{ij}^f},
\tag{4}
$$

where the χs are dimensionless and constrained by flavour physics experimental data, which will be discussed in the following section. Then, one can obtain the generic Lagrangian of the Yukawa sector, which gives the interactions of physical (pseudo)scalars fields with fermions, as:[3]

$$
\mathcal{L}^{\bar{f}_i f_j \phi} = -\left\{ \frac{\sqrt{2}}{v}\bar{u}_i\big(m_{d_j} X_{ij} P_R + m_{u_i} Y_{ij} P_L\big)d_j H^+ \right.
$$

$$
\left. + \frac{\sqrt{2}m_{l_j}}{v} Z_{ij}\bar{\nu}_L l_R H^+ + h.c.\right\}
$$

$$
- \frac{1}{v}\left\{ \bar{f}_i m_{f_j} h_{ij}^f f_j h^0 - i\,\bar{f}_i m_{f_i} A_{ij}^f f_j \gamma_5 A^0\right\},
\tag{5}
$$

where X_{ij}, Y_{ij}, Z_{ij}, A_{ij} are given in [16]. For our study it is sufficient to consider the functions h_{ij}^f, which are given by:

$$
h_{ij}^u = \varepsilon_h^u \delta_{ij} - \frac{(\varepsilon_H^u + Y\varepsilon_h^u)}{\sqrt{2}f(Y)}\sqrt{\frac{m_{u_j}}{m_{u_i}}}\chi_{ij}^u,
\tag{6}
$$

$$
h_{ij}^d = \varepsilon_h^d \delta_{ij} + \frac{(\varepsilon_H^d - X\varepsilon_h^d)}{\sqrt{2}f(X)}\sqrt{\frac{m_{d_j}}{m_{d_i}}}\chi_{ij}^d,
\tag{7}
$$

wherein the parameters $X, Y, \varepsilon_{h,H}^{u,d}$ are given in Table 1, where it is made clear that our 2HDM-III construct with a four-zero Yukawa texture can be related to the ordinary Yukawa types known as Type I, II and Y (or flipped) by choosing appropriately these parameters.

In general, the Higgs-fermion–fermion couplings are expressed as $g_{2\text{HDM-III}}^{ff\phi} = g_{\text{any}}^{ff\phi} + \Delta g$, where $g_{\text{any}}^{ff\phi}$ represents the $ff\phi$ coupling in any 2HDM with a discrete symmetry and Δg is the contribution of the four-zero texture [16].

3 Constraints and benchmark scenarios

In previous works [11,16,40,45], we have constrained our model by considering EWPOs, flavour and Higgs physics constraints from experimental data as well as theoretical bounds (such as unitarity [46,47], vacuum stability [48,49] and perturbativity). Since the theoretical bounds and EWPO constraints have been analysed very recently [50], and these have not changed, we refer the reader to such a paper. In contrast, experimental constraints evolve continuously so here we have re-evaluated them in the light of the very latest results. Specifically, the parameter space of the model was constrained by flavour physics measurements, through the experimental data bounds from leptonic and semileptonic meson decays, the inclusive decay $B \to X_s\gamma$, the $B_0 - B_0$ and $K_0 - K_0$ mixing as well as the process $B_s \to \mu^+\mu^-$ [16,51]. We have then used HiggsBounds [39,52] and HiggsSignals [53,54] to place bounds over the masses and couplings of neutral [55,56] and charged Higgs bosons [57–62], so as to make sure that the parameter space of the 2HDM-III considered here is consistent with any Higgs boson searches

---

[3] One can assume this Lagrangian is the one of an effective field theory, wherein the Higgs fields play a relevant role in the flavour structure of some high scale renormalisable flavour model [41–44].

Table 2 Values for free parameters which define our benchmark scenarios, all being consistent with current theoretical and experimental bounds

Scenario	$\cos(\beta - \alpha)$	$\chi^u_{\{22,23,33\}}$	$\chi^d_{\{22,23,33\}}$	$\chi^l_{\{22,23,33\}}$
Ia	0.1	$\{1, 0.1, 1.4\}$	$\{1.8, 0.1, 1.2\}$	$\{-0.4, 0.1, 1\}$
IIa	0.1	$\{1, -0.53, 1.4\}$	$\{1.8, 0.2, 1.3\}$	$\{-0.4, 0.1, 1\}$
Y	0.1	$\{1, -0.53, 1.4\}$	$\{1.8, 0.2, 1.3\}$	$\{-0.4, 0.1, 1\}$
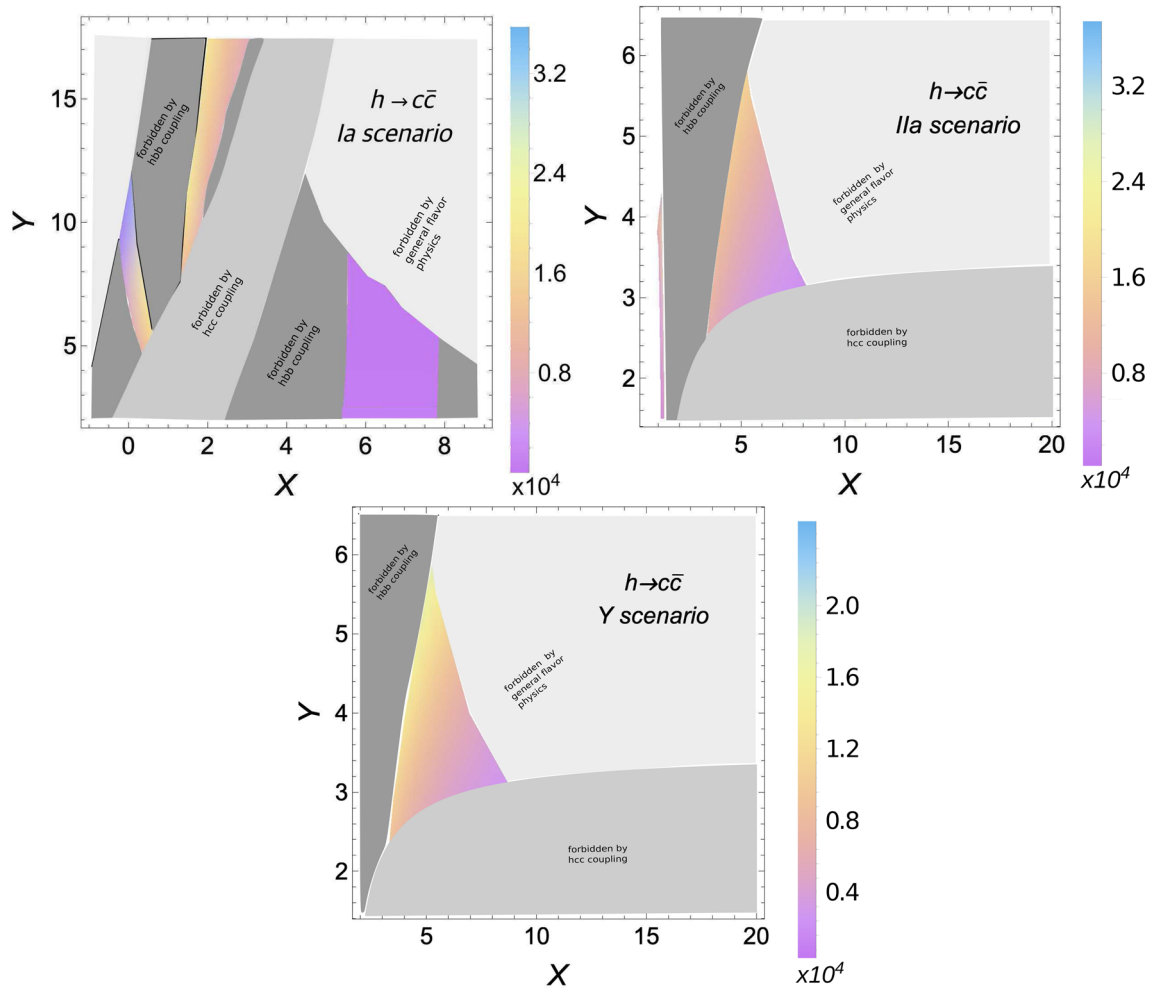
Fig. 1 Event rates for each benchmark scenario over the (X, Y) plane computed as $\sigma(ep \to \nu_e hj) \times \mathrm{BR}(h \to c\bar{c}) \times \epsilon_c^2 \times 1$ ab^{-1}. Here, we have $E_p = 50$ TeV and $E_{e^-} = 60$ GeV (with $P_L^{e^-} = -80\%$)

and measurements conducted at the LHC and previous colliders. In particular, using LHC measurements of the SM-like Higgs boson in the decays $h \to \gamma\gamma$ and γZ [54,63–67], we made sure that the Yukawa texture involving the couplings of the charged Higgs boson with fermions in the loops of these processes is in agreement with data. Specifically, in the permitted region of parameter space of our model, rather low masses for the charged Higgs bosons are allowed [30,45,50,68].

As intimated, in this study, the scalar field h is the SM-like Higgs boson, hence, $m_h = 125$ GeV. Furthermore, we choose the following parameter space: $m_A = 150$ GeV, 125

GeV $< m_H < 200$ GeV, 100 GeV $< m_{H^\pm} < 170$ GeV and $\cos(\beta - \alpha) \approx 0.1$, with $0.014 \leq S \leq 0.026$ and $-0.02 \leq T \leq 0.028$ and tensioned these against the measured values $S = -0.010.07$ and $T = 0.040.06$ (fixing $U = 0$) taken from [69], being all this parameter space consistent with the aforementioned theoretical conditions and experimental data. Then, we select some sets of free parameters χ's which will represent our benchmark scenarios for each of the discussed 2HDM-III realisations (or incarnations). Explicitly, these benchmark scenarios are shown in Table 2. We have characterised these benchmark scenarios in Fig. 1, where we show the events rates for the aforemen-

Table 3 Relevant cross sections, BRs and event rates (for the machine configuration given in the previous figure caption) for our scenarios Ia, IIa and Y, each mapped in terms of X, Y and Z values. We have included the allowed values for μ and κ_c for each BPs. Here, we have included the following tagging efficiencies in the last column: $\epsilon_b = 0.6$, $\epsilon_c = 0.24$ and $\epsilon_s = 0.05$ [77]

Point	$X(Z)$	Y	BR($\phi^0 \to ab$)	$\sigma(e^- p \to e^- \phi^0 q)$	Events (1 ab^{-1})
			BR($h \to b\bar{b}$) = 0.513		2×10^5
Ia	0.5 (0.5)	6.5	BR($h \to c\bar{c}$) = 0.484		2×10^4
	$\mu = 0.88$		BR($h \to sb$) = 1.99×10^{-3}	0.875 pb	52
	$\kappa_c = 1.5$		BR($h \to s\bar{s}$) = 8.18×10^{-9}		0
			BR($h \to b\bar{b}$) = 0.67		2×10^5
IIa	1 (1)	4	BR($h \to c\bar{c}$) = 0.23	0.958 pb	2×10^4
	$\mu = 1.16$		BR($h \to sb$) = 0.093		1×10^3
	$\kappa_c = 2$		BR($h \to s\bar{s}$) = 2.87×10^{-3}		7
			BR($h \to b\bar{b}$) = 0.498		2×10^5
Y-min	5 ($-1/5$)	5	BR($h \to c\bar{c}$) = 0.289	1.08 pb	2×10^4
	$\mu = 0.86$		BR($h \to sb$) = 0.21		7×10^3
	$\kappa_c = 1.7$		BR($h \to s\bar{s}$) = 1.96×10^{-3}		5

tioned production and decay process over the (X, Y) plane for case Ia, IIa and Y of Table 2. These events rates are realised at parton level, taking the efficiency of c-tagged jets as $\epsilon_c = 0.24$ and assuming 1 ab^{-1} of (integrated) luminosity. The coloured regions over the (X, Y) plane shown herein are compliant with all aforementioned constraints while the white backgrounds correspond to regions ruled out. Furthermore, we have demanded that for all benchmark points the BR($h \to b\bar{b}$) is in agreement with the latest experimental observations, which established as ratio of the measured value to the SM prediction the following one $\mu = 1.04 \pm 0.20$ [70–72]. Moreover, we have considered the most recent and stringent direct constraint for the Higgs-charm Yukawa coupling modifier κ_c obtained by CMS and ATLAS [73,74], where $1.1 < |\kappa_c| < 5.5$ and this one is interpreted in the κ-framework [75,76]. These last constraints are responsible for the absence of continuity across all allowed regions. This is due to the fact that the Yukawa couplings are strongly sensitive to the X and Y values, hence the BR($h \to b\bar{b}$) is too, as well as BR($h \to c\bar{c}$). For example, for the Ia scenario, over the region with $2 < X < 5$, the BR($h \to b\bar{b}$) is above the mentioned experimental bounds but, if Y grows larger, $h \to c\bar{c}$ starts to be relevant and the BR($h \to b\bar{b}$) decreases until acceptable values. In contrast, in the region $0 < X < 1$, the channel $h \to b\bar{b}$ is generally inconsistent with experimental data unless Y is small, so that the $h \to c\bar{c}$ decay rate is small too and the BR($h \to b\bar{b}$) is within the allowed limits from the experimental data connected at the CERN machine.

The discussed event rates are calculated via the formula $\sigma(ep \to \nu_e hj) \times$ BR($h \to c\bar{c}$) $\times$ 1 ab^{-1} $\times \epsilon_c^2$ (as mentioned, we take $\epsilon_c = 0.24$ as an approximation of the efficiency of a standard c-tagging algorithm suitable for the FCC-eh environment [77]). The cross sections and BRs have been

calculated using CalcHEP 3.7.5 [78], wherein the 2HDM-III has been implemented by ourselves. The proton beam is taken with 50 TeV of energy (E_b), assuming CTEQ6L1 as Parton Distribution Functions (PDFs) [79], while the electron beam is considered to be of 60 GeV (E_{e^-}) with a (longitudinal) polarisation ($P_L^{e^-}$) of -80% [80]. For each of these BPs we give herein the common cross section, the BRs into $b\bar{b}$, $c\bar{c}$, $s\bar{b}$ plus Charge Conjugate (C.C.) and $s\bar{s}$.

As prospect of our work, for ee-colliders as ILC [81] (CLIC [82]) machine the cross sections of Higgs production would be $\sigma(e^+e^- \to \nu_e \bar{\nu}_e h) \sim 220$ fb (~ 600 fb) and the main cross section $\sigma(e^- p \to hj\nu_e) \sim 190$ fb ($\sim 1000 fb$) for electron proton-colliders LHeC (FCC-he), with center-of mass energy of $\sqrt{s} = 1.3$TeV ($\sqrt{s} = 3.5$ TeV) . One can see, the cross sections are the same order of magnitude. Therefore, the studies of Higgs factories would be complement among ee-colliders and ep- colliders.

4 Numerical analysis

The first step of our numerical analysis is to compare the production and decay rate of signal events to those of the various backgrounds, in presence of acceptance and selection cuts. The latter are implemented at the parton level as $p_T(q) > 10$ GeV, $\Delta R(q, q) > 0.3$ and $|\eta(q)| < 7$, where q represents any quark involved. For our Signal (S), we refer to the inclusive rates in Table 3. For the Background (B), final states of the type $\not{E}_T + 3$ jet are considered. In order to not overload with information the forthcoming histograms, we consider the following five compounded contributions (wherein j represents any jet except a b-one): $\nu 3j$ (it represents the set of $\nu_e jjj$, $\nu_e bjj$ and $\nu_e bbj$ final states), $\nu_e llj$

Table 4 Background cross sections and event rates at parton level after the following cuts: $p_T(q) > 10$ GeV, $\Delta R(q, q) > 0.3$ and $|\eta(q)| < 7$ (assuming the usual FCC-eh parameters)

Background	Cross section [pb]	Number of events
$\nu_e jjj$	172	1.75×10^8
$\nu_e bjj$	16.1	1.61×10^7
$\nu_e bbj$	1.8	1.8×10^6
$\sum \nu 3j$	189.9	10^8
$\nu_e llj$	3.09	3.09×10^6
$\nu_e tb$	12.47	1.24×10^7
$ejjj$	948	9.48×10^8
$ebjj$	17.8	1.78×10^7
$ebbj$	75.4	75.4×10^7
$\sum ejjj$	1040	10^9
ett	0.35	3.5×10^5

(for any configuration of charged leptons and quarks), $\nu_e tb$, $e3j$ (for $ejjj$, $ebjj$ and $ebbj$) and ett. In Table 4, one can see the corresponding cross sections at parton level for all these backgrounds as well as the corresponding event rates for the usual FCC-eh parameters.

For the analysis at detector level, we proceed in the following way: we use PYTHIA8 [83] as parton shower and hadronisation generator and Delphes [84] as detector simulator. Delphes was run via a FCC-eh card provided in [85]. Finally, we employed MadAnalysis5 [86] to construct histograms and implement the event selections.

In order to reconstruct the final state of interest, enriched by two c-jets, we need to worry about the presence of b-jets, as both c- and b-quarks will originate jets with displaced vertices: thus, just like there is a non-zero probability of b-jets being tagged as c-jets also the vice versa is possible. Furthermore, a value of 60% for ϵ_b essentially means that some b-jets (precisely, 40% of them) could be tagged as either c-jet or lighter ones.[4] In essence, it is not obvious what will be the number of true $c\bar{c}$ events in the complete di-jet sample (although this is all modelled by Delphes). However, in order to extract the $hc\bar{c}$ vertex strength, we can proceed as follows. To start with, the portion of $b\bar{b}$ events recognised as such, $N_b \approx \epsilon_b^2$, can be filtered out. Conversely, around $1 - \epsilon_b^2$ of $b\bar{b}$ events would be accounted as light di-jets ones (including $c\bar{c}$ ones, that we do not separate out), which we label as $N_{b\to j}$. (In fact, the latter also includes a $\propto (1 - \epsilon_b)$ subleading contribution from mistagged $s\bar{b}$ + C.C. events.) This will add to the true number of events with only light jets, N_j, where $j = s$. Likewise, the portion of $c\bar{c}$ events recognised as such is $N_c = \epsilon_c^2$, which in turn implies that $1 - \epsilon_c^2$ of these will appear as light jets, labelled as $N_{c\to j}$. These will

also add to the N_j rate alongside the $N_{b\to j}$ one. In order to perform an unbiased measurement of the Yukawa coupling $hc\bar{c}$ we can only rely on the N_c sample. However, we can use the sample constituted by $N_j + N_{b\to j} + N_{c\to j}$ di-jet events, wherein it is not necessary to extract the fraction of b-jets appearing as c-jets, for validation purposes, to ensure that the two measurements are consistent with each other, so that, in the remainder of our analysis, we will consider the two cases in parallel.[5]

Now, having defined two di-jet samples accounting for flavour (mis)tagging effects, in order to remove the contamination from backgrounds having kinematic configurations similar to the signals, irrespectively of the flavour composition, we proceed by enforcing the following sets of cuts. (Notice that the kinematics of any h decay into di-jets is the same, given the much larger value of $m_h = 125$ GeV with respect to any m_q with $q = d, u, s, c$ and b.)

A) We impose the following initial conditions for jets and leptons: $p_T(j) > 10$ GeV, $p_T(l) > 10$ GeV and $|\eta(j)| < 6$. Once these requirements are combined with the described tagging procedure, we have events composed of missing (transverse) energy and three jets.

B) From the left histogram of Fig. 2, one can select the most relevant signature in terms of jet multiplicity, specifically, we select events with exactly two jets. In fact, the third jet typically comes directly from the primary vertex and is very forward, when not outside the detection zone (i.e., $|\eta(j_3)| > 6$), therefore it is not considered in our analysis. Furthermore, for any jet multiplicity $N[j] > 3$, the signal yield is far too depleted to be of numerical interest. Another cut is over the missing (transverse) energy, as we take $E_T > 30$ GeV (see the histogram on the right-hand side of Fig. 2). Specifically, this cut is very strong against the $ejjj$ background, as it keeps only around 20% of such events without penalising the signals excessively.

C) The third set of cuts are imposed over the pseudorapidity and transverse momentum of each jet. To start with, we use η ordering to tag the first or second jet (i.e., $|\eta(j_1)| > |\eta(j_2)|$). About pseudorapidity, we demand $\eta(j_1) < -3.5$ and $\eta(j_2) < -4$. These cuts are highly restrictive onto $ejjj$ and νjjj, keeping around of 8% and 50% of these events, respectively (see top histograms in Fig. 3). Furthermore, the selections in jet transverse momentum are $p_T(j_1) < 90$ GeV, which has a strong impact on the $ejjj$ and ett backgrounds, and $p_T(j_2) > 30$ GeV, which affects mainly the νjjj and νtb noises (see bottom histograms in Fig. 3).

---

[4] We neglect here the possibility of s-jets to be tagged as c- or b-ones, so that we need not worry about the role of $s\bar{b}$ + C.C. and $s\bar{s}$ events.

[5] This search technique of $hc\bar{c}$ coupling can be employed for the nearer future Large Hadron-electron Collider (LHeC).
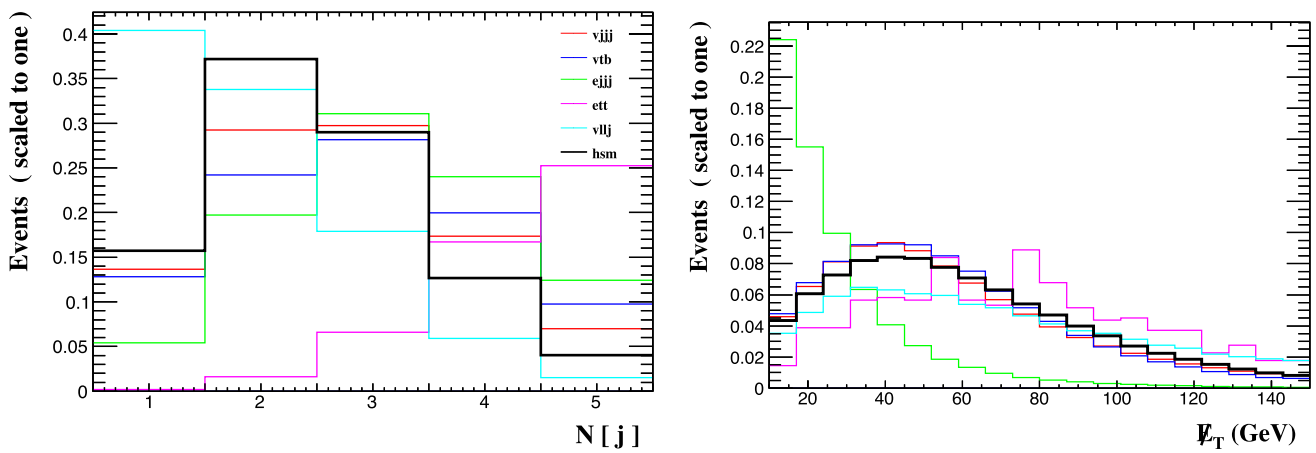
Fig. 2 (Left) jet multiplicity (whichever their flavour) distribution. (Right) missing (transverse) energy distribution. These histograms are made for the Ia incarnation of the 2HDM-III signal as well as the five categories of background discussed in the text
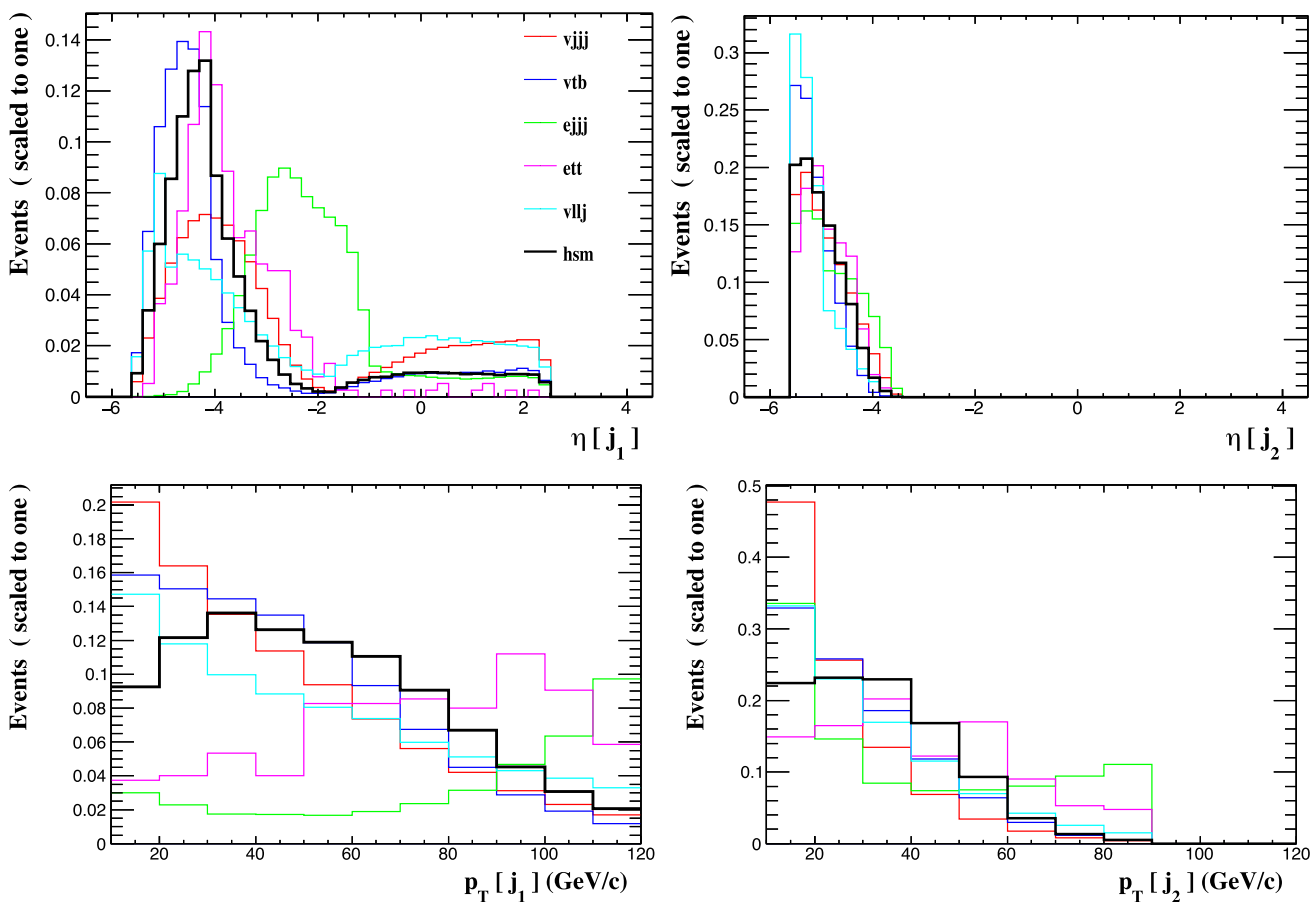

Fig. 3 (Top-left) jet pseudorapidity distribution for the first jet. (Top-right) same for the second jet. (Bottom-left) transverse momentum distribution for the first jet. (Bottom-right) same for the second jet. These histograms are made for the Ia incarnation of the 2HDM-III signal as well as the five categories of background discussed in the text

D) We impose that $\Delta R(j_1, j_2) \equiv \sqrt{\Delta\phi(j_1, j_2)^2 + \Delta\eta(j_1, j_2)^2} > 1.6$. This cut enhances the signal above all backgrounds except $ejjj$: see Fig. 4.

E) Finally, we impose a selection on invariant mass for of the two jets, which are the candidates to reconstruct the SM-like Higgs boson mass. Specifically, this cut is 100 GeV $< M(j_1, j_2) < 125$ GeV: see Fig. 5.
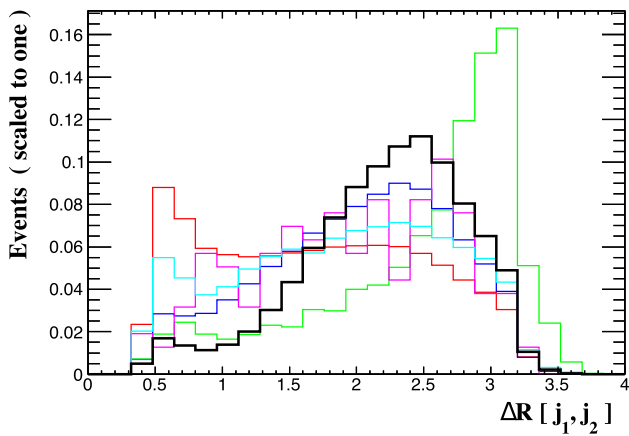
Fig. 4 Jet separation distribution. These histograms are made for the Ia incarnation of the 2HDM-III signal as well as the five categories of background discussed in the text

(Notice that we have illustrated the kinematics of the Ia incarnation of the 2HDM-III signal but we can confirm that results are extremely similar for the IIa and Y cases as well.)

The response of all signals and backgrounds to each of the above cuts is captured in Table 5. Here, the top value in each row represents the signal rate with no flavour being filtered, i.e., this is the effective di-jet final state defined above as $N_j + N_{b \to j} + N_{c \to j}$ while the bottom value is the estimated number of N_c events made up by $c\bar{c}$ pairs recognised as such. It is clear that the kinematic selection is effective in significantly reducing all of the latter without greatly affecting all of the former. This is well exemplified by the values of the final S versus B rates, including the significances, defined as $\frac{S}{\sqrt{S+B}}$. The fact that the corresponding values are always well beyond 5, whichever flavour tagging, clearly indicates the discovery potential of both $h \to jj$ and $h \to c\bar{c}$ events at the FCC-eh with a confidence level against the possibility of a background fluctuation far higher than at any hadron collider foreseen at CERN, i.e., a HL-LHC and FCC-hh [20,24], and comparable to that of the FCC-ee [87], a future e^+e^- collider therein.
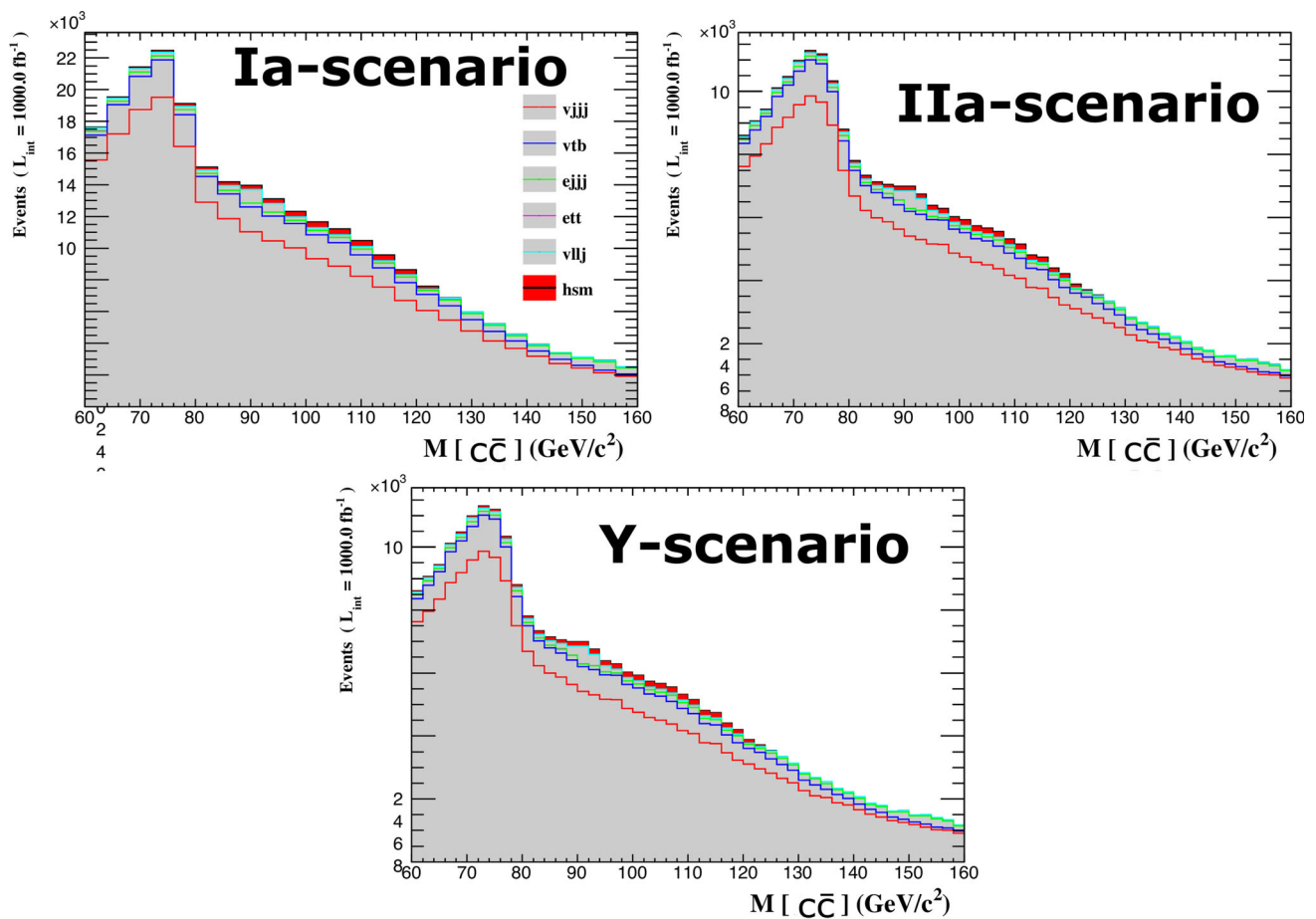

Fig. 5 Di-jet invariant mass distribution. These histograms are made for the Ia (top-left), IIa (top-right) and Y (bottom) incarnations of the 2HDM-III signal (red histogram) as well as the five categories of background discussed in the text (here stacked beneath the signal). Here, we present the rates for the case of $c\bar{c}$-tagged sample

Table 5 Cutflow for all signals and backgrounds. Here, in each cell, the top line represents the number of light di-jet events while the bottom one refers to those enriched by $c\bar{c}$ states, as described in the text

Signal	Raw events	Sim events	Set A)	Set B)	Set C)	Set D)	Set E)	Significance
Ia	875,000	890,530	633,866	190,986	91,117	77,079	36,054	36.3
			36,075	10,869	5186	4387	2052	8.31
IIa	958,000	970,336	609,152	178,088	87,714	72,312	30,898	31.19
			32,350	9457	4658	3840	1641	6.67
Y	1,070,000	1,085,244	736,138	208,665	101,427	83,083	35,824	36.08
			41,941	11,884	5776	4732	2040	8.27
$\Sigma v 3j$	1.89×10^8	19,956,113	176,368,197	40,956,844	9,327,890	4,960,087	820,718	
			10,334,771	2,399,977	546,593	290,650	48,092	
vtb	1.24×10^7	1,254,485	7,880,059	1,505,048	759,201	548,492	123,961	
			501,285	95,743	48,296	34,892	7886	$\Sigma B =$
$\Sigma e 3j$	10^9	10,4495,242	73,393,857	3,093,729	29,137	24,770	2750	950,207
			52,792,574	2,225,334	20,958	17,817	1978	58,865
ett	350,000	353,583	26,046	380	109	77	21	
			14,764	215	62	44	12	
$\Sigma v llj$	3,090,000	1,434,318	411,923	117,562	29,915	19,052	2757	
			134,029	38,253	9733	6199	897	

5 Conclusions

In summary, we have studied the process $e^- p \rightarrow v_e h q$ assuming the decay channel $h \rightarrow c\bar{c}$, where h is the discovered SM-like state, at a FCC-eh with $E_b = 50$ TeV and $E_{e^-} = 60$ GeV in presence of a -80% polarisation of the e^- beam. We considered this channel in the context of a 2HDM-III embedding a four-zero texture in the Yukawa matrices and a general Higgs potential, where both Higgs doublets are coupled with up- and down-type fermions, as a theoretical framework that can be mapped into the standard four types of 2HDM. Hence, we have defined three limits of it reproducing the Type I, II and Y (but not X, which offers no sensitivity to our study) setups. The purpose was to show that this collider has the ability to access the Yukawa coupling between the SM-like Higgs state and c-quarks, which can only be determined with significant errors at present and future hadronic machines, like the (HL-)LHC and FCC-hh.

Upon accounting for flavour mistagging effects in a realistic way in presence of parton shower, hadronisation and detector effects and simulating both reducible and irreducible backgrounds, we have proven that large significances can be achieved at such FCC-eh, above and beyond what attainable at the aforementioned hadronic machines and comparable to the FCC-ee expectations. This conclusion applies to all three 2HDM-III incarnations discussed, each being exemplified by two BPs at the edges of the currently allowed (by LHC data) interval on the Yukawa coupling between the SM-like Higgs state and b-quarks.

Data Availability Statement This manuscript has no associated data or the data will not be deposited. [Authors' comment: All results are documented using the arXiv metadata repository. Research data from this work has been submitted to arXiv and is available to the international physics community and the general public. The data are results of numerical calculations considering theoretical and analytical computations. All calculations were done with high energy physics tools and mathematical.]

References

1. S. Moretti, W. J. Stirling, Phys. Lett. B **347**, 291 (1995) [Erratum: Phys. Lett. B 366, 451 (1996)]
2. S.-Y. Li, Z.-Y. Li, P.-C. Lu, Z.-G. Si, Chin. Phys. C **45**, 093105 (2021)
3. G.C. Branco, P.M. Ferreira, L. Lavoura, M.N. Rebelo, M. Sher, J.P. Silva, Phys. Rep. **516**, 1 (2012)
4. V.D. Barger, J.L. Hewett, R.J.N. Phillips, Phys. Rev. D **41**, 3421 (1990)
5. Y. Grossman, Nucl. Phys. B **426**, 355 (1994). arXiv:hep-ph/9401311
6. M. Aoki, S. Kanemura, K. Tsumura, K. Yagyu, Phys. Rev. D **80**, 015017 (2009). arXiv:0902.4665 [hep-ph]
7. J.F. Gunion, H.E. Haber, G.L. Kane, S. Dawson, Front. Phys. **80**, 1–425 (2000)
8. J.F. Donoghue, L.F. Li, Phys. Rev. D **19**, 945 (1979)
9. R.M. Barnett, G. Senjanovic, D. Wyler, Phys. Rev. D **30**, 1529 (1984)
10. H. Fritzsch, Z.-Z. Xing, Phys. Lett. B **555**, 63 (2003)
11. J.L. Diaz-Cruz, J. Hernandez-Sanchez, S. Moretti, R. Noriega-Papaqui, A. Rosado, Phys. Rev. D **79**, 095025 (2009)
12. J. Hernández-Sánchez, O. Flores-Sánchez, C. G. Honorato, S. Moretti, S. Rosado, PoS CHARGED2016 **032**, 1–6 (2017)
13. J. Hernandez-Sanchez, S. Moretti, R. Noriega-Papaqui, A. Rosado, PoS CHARGED2012 **029**, 1–6 (2012)
14. J. Hernandez-Sanchez, S. P. Das, S. Moretti, A. Rosado, R. Xoxocotzi-Aguilar, PoS DIS2015 **227**, 1–6 (2015)
15. S.P. Das, J. Hernández-Sánchez, S. Moretti, A. Rosado, R. Xoxocotzi, Phys. Rev. D **94**, 055003 (2016)
16. J. Hernandez-Sanchez, S. Moretti, R. Noriega-Papaqui, A. Rosado, JHEP **07**, 044 (2013)
17. A.G. Akeroyd et al., Eur. Phys. J. C **77**, 276 (2017)
18. A.G. Akeroyd, S. Moretti, J. Hernandez-Sanchez, Phys. Rev. D **85**, 115002 (2012)
19. F. Gianotti et al., Eur. Phys. J. C **39**, 293 (2005)
20. G. Apollinari, I. Béjar Alonso, O. Brüning, P. Fessia, M. Lamont, L. Rossi, L. Tavian, CERN- 2017-007-M 4/2017 (2017)
21. M. Kuze, Int. J. Mod. Phys. Conf. Ser. **46**, 1860081 (2018)
22. D. Britzger, M. Klein, PoS DIS2017 **105**, 1–24 (2018)
23. A. Abada et al. (FCC), Eur. Phys. J. C **79**, 474 (2019)
24. A. Abada et al. (FCC), Eur. Phys. J. ST **228**, 755 (2019)
25. A. Jueid, J. Kim, S. Lee, J. Song, Phys. Lett. B **819**, 136417 (2021)
26. H.E. Haber, R. Hempfling, Phys. Rev. D **48**, 4280 (1993). arXiv:hep-ph/9307201
27. J.F. Gunion, H.E. Haber, Phys. Rev. D **67**, 075019 (2003)
28. M.N. Dubinin, A.V. Semenov, Eur. Phys. J. C **28**, 223 (2003). arXiv:hep-ph/0206205
29. J.F. Gunion, H.E. Haber, Phys. Rev. D **72**, 095002 (2005). arXiv:hep-ph/0506227
30. A. Cordero-Cid, J. Hernandez-Sanchez, C.G. Honorato, S. Moretti, M.A. Perez, A. Rosado, JHEP **07**, 057 (2014)
31. J.M. Gerard, M. Herquet, Phys. Rev. Lett. **98**, 251802 (2007)
32. D. Toussaint, Phys. Rev. D **18**, 1626 (1978)
33. S. Bertolini, Nucl. Phys. B **272**, 77 (1986)
34. W. Hollik, Z. Phys. C **32**, 291 (1986)
35. J.F. Gunion, A. Turski, Phys. Rev. D **39**, 2701 (1989)
36. S. de Visscher, J.-M. Gerard, M. Herquet, V. Lemaitre, F. Maltoni, JHEP **08**, 042 (2009)
37. J. Haller, A. Hoecker, R. Kogler, K. Mönig, T. Peiffer, J. Stelzer, Eur. Phys. J. C **78**, 675 (2018)
38. S. Kanemura, Y. Okada, H. Taniguchi, K. Tsumura, Phys. Lett. B **704**, 303 (2011)
39. P. Zyla et al. (Particle Data Group), PTEP **2022**(8), 083C01 (2022). https://doi.org/10.1093/ptep/ptac097
40. O. Félix-Beltrán, F. González-Canales, J. Hernández-Sánchez, S. Moretti, R. Noriega-Papaqui, A. Rosado, Phys. Lett. B **742**, 347 (2015)
41. A. Aranda, C. Bonilla, A.D. Rojas, Phys. Rev. D **85**, 036004 (2012)
42. G. Branco, D. Emmanuel-Costa, C. Simões, Phys. Lett. B **690**, 62 (2010)
43. F. Botella, G. Branco, M. Rebelo, Phys. Lett. B **722**, 76 (2013)
44. M. Frigerio, S. Kaneko, E. Ma, M. Tanimoto, Phys. Rev. D **71**, 011901 (R) (2005)
45. A. Cordero-Cid, J. Hernádez-Sánchez, C. Honorato, S. Moretti, PoS Charged **2014**, 026 (2015)
46. R. Casalbuoni, D. Dominici, R. Gatto, C. Giunti, Phys. Lett. B **178**, 235 (1986)
47. I.F. Ginzburg, I.P. Ivanov, Phys. Rev. D **72**, 115010 (2005). arXiv:hep-ph/0508020
48. P.M. Ferreira, R. Santos, A. Barroso, Phys. Lett. B **603**, 219 (2004) [Erratum: Phys.Lett.B 629, 114–114 (2005)]. arXiv:hep-ph/0406231
49. I.P. Ivanov, Phys. Rev. D **77**, 015017 (2008). arXiv:0710.3490 [hep-ph]
50. J. Hernández-Sánchez, C.G. Honorato, S. Moretti, S. Rosado-Navarro, Phys. Rev. D **102**, 055008 (2020)
51. A. Crivellin, C. Greub, A. Kokulu, Phys. Rev. D **87**, 094031 (2013)
52. G. Aad et al. (ATLAS), Phys. Rev. D **101**, 012002 (2020)
53. G. Aad et al. (ATLAS, CMS), JHEP **08**, 045 (2016)
54. A.M. Sirunyan et al. (CMS), Eur. Phys. J. C **79**, 421 (2019)
55. A.M. Sirunyan et al. (CMS), JHEP **03**, 055 (2020)
56. V. Khachatryan et al. (CMS), Phys. Lett. B **759**, 369 (2016)
57. G. Abbiendi et al. (ALEPH, DELPHI, L3, OPAL, LEP), Eur. Phys. J. C **73**, 2463 (2013)
58. B. Abbott et al. (D0), Phys. Rev. Lett. **82**, 4975 (1999)
59. A. Abulencia et al. (CDF), Phys. Rev. Lett. **96**, 042003 (2006)
60. V.M. Abazov et al. (D0), Phys. Lett. B **682**, 278 (2009)
61. A.M. Sirunyan et al. (CMS), JHEP **11**, 115 (2018). arXiv:1808.06575 [hep-ex]
62. A.M. Sirunyan et al. (CMS), JHEP **07**, 142 (2019)
63. M. Aaboud et al. (ATLAS), Phys. Lett. B **784**, 345 (2018)
64. M. Aaboud et al. (ATLAS), Phys. Lett. B **786**, 114 (2018)
65. G. Aad et al. (ATLAS), Phys. Lett. B **809**, 135754 (2020)
66. M. Aaboud et al. (ATLAS), JHEP **10**, 112 (2017)
67. A.M. Sirunyan et al. (CMS), JHEP **11**, 152 (2018)
68. O. Flores-Sánchez, J. Hernández-Sánchez, C.G. Honorato, S. Moretti, S. Rosado-Navarro, Phys. Rev. D **99**, 095009 (2019)
69. R.L. Workman et al. (Particle Data Group), PTEP 2022 **083C01** (2022)
70. A. Sopczak (ATLAS, CMS), PoS FFK2019 **006** (2020)
71. M. Aaboud et al. (ATLAS), Phys. Lett. B **786**, 59 (2018)
72. A.M. Sirunyan et al. (CMS), Phys. Rev. Lett. **121**, 121801 (2018)
73. G. Aad et al. (ATLAS), Eur. Phys. J. C **82**, 717 (2022). arXiv:2201.11428 [hep-ex]
74. (2022) arXiv:2205.05550 [hep-ex]
75. J.R. Andersen et al. (LHC Higgs Cross Section Working Group), (2013). https://doi.org/10.5170/CERN-2013-004. arXiv:1307.1347 [hep-ph]
76. D. de Florian et al. (LHC Higgs Cross Section Working Group), **2/2017** (2016). https://doi.org/10.23731/CYRM-2017-002. arXiv:1610.07922 [hep-ph]
77. U. Klein et al., in *Meeting of the Physics Convenors of the LHeC, Higgs at LHeC/FCC-he conferences* (2014). https://indico.cern.ch/event/350727/contributions/826001/attachments/693294/
78. A. Belyaev, N.D. Christensen, A. Pukhov, Comput. Phys. Commun. **184**, 1729 (2013). arXiv:1207.6082 [hep-ph]
79. J. Pumplin, D.R. Stump, J. Huston, H.L. Lai, P.M. Nadolsky, W.K. Tung, JHEP **07**, 012 (2002)
80. P. Agostini et al. (LHeC, FCC-he Study Group), JLAB-ACP-20-3180 (2020)

81. H. Aihara et al. (ILC), (2019). arXiv:1901.09829 [hep-ex]
82. **4/2018** (2018). https://doi.org/10.23731/CYRM-2018-004. arXiv:1903.08655 [physics.acc-ph]
83. T. Sjöstrand, S. Ask, J.R. Christiansen, R. Corke, N. Desai, P. Ilten, S. Mrenna, S. Prestel, C.O. Rasmussen, P.Z. Skands, Comput. Phys. Commun. **191**, 159 (2015). https://doi.org/10.1016/j.cpc.2015.01.024. arXiv:1410.3012 [hep-ph]
84. J. de Favereau, C. Delaere, P. Demin, A. Giammanco, V. Lemaître, A. Mertens, M. Selvaggi (DELPHES 3), JHEP **02**, 057 (2014)
85. U. Klein et al., Final FCChe delphes card and discussion, Higgs and Top at LHeC conferences. (2017). https://indico.cern.ch/event/624658/
86. E. Conte, B. Fuks, G. Serret, Comput. Phys. Commun. **184**, 222 (2013). arXiv:1206.1599 [hep-ph]
87. A. Abada et al. (FCC), Eur. Phys. J. ST **228**, 261 (2019)